Journal of Power Sources 270 (2014) 536–546

Contents lists available at ScienceDirect

Journal of Power Sources

journal homepage: www.elsevier.com/locate/jpowsour

Pore network design: DPD-Monte Carlo study of solvent diffusion dependence on side chain location

Gert Dorenbos*

Sano 1107-2, Belle Crea 502, Susono-shi, Shizuoka-ken 410-1118, Japan

HIGHLIGHTS

- Morphologies within amphiphilic membranes are modeled by dissipative particle dynamics.
- Polymer backbones are hydrophobic and side chains have a pendant hydrophilic end moiety.
- Hydration levels and ion exchange capacity are kept fixed.
- Water diffusion is obtained from (1) Monte Carlo tracer diffusion and (2) water bead motion.
- Enhanced diffusion occurs when two side chains are branching off from single backbone sites.

GRAPHICAL ABSTRACT

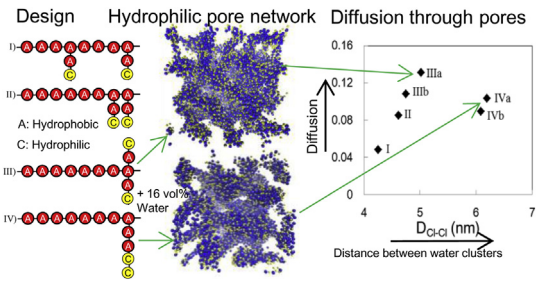

ARTICLE INFO

Article history:
Received 8 March 2014
Received in revised form
22 July 2014
Accepted 23 July 2014
Available online 1 August 2014

Keywords:
Membrane
Chain architecture
Phase separation
Simulation
Diffusion
Fuel cell

ABSTRACT

Phase separation within water containing polymer membranes is studied by dissipative particle dynamics (DPD). The polymers are composed of hydrophobic backbone A beads to which ([A-C] or [A-A-C-C]) side chains are attached with a hydrophilic (C) end moiety. Water diffusion through the water containing pores is modeled by Monte Carlo (MC) tracer diffusion. Several polymeric architectures are considered which differ in the way side chains are attached along the polymer backbones. In total 120 pore morphologies are stored on file and probed by MC tracer diffusion calculations. For membranes of the same ion exchange capacity diffusion is highest for architectures for which two side chains are branching off from the backbone sites as compared to architectures for which only one side chain is branching off. This conclusion is also obtained from diffusion constants derived from mean squared displacements of water during the DPD simulations. The intrinsic high polymer mobility in conventional DPD results in water diffusivities that are much higher than those obtained from the MC calculations. Assigning higher masses to the polymer beads results in significant decrease in water bead motion.

© 2014 Published by Elsevier B.V.

1. Introduction

Nafion® is applied in water purification by reverse osmosis [1], dialysis and as a proton exchange membrane (PEM) in polymer electrolyte fuel cells (PEFC). Within a PEM Nafion separates the cathode from the anode and simultaneously acts as a conductor for protons. The chemical formula of Nafion is given in Fig. 1(a). Nafion is a per-fluorinated sulfonic acid (PFSA) ionomer that has side chains attached to its hydrophobic Teflon ($-CF_2-$) backbone. Since the side chains contain pendant hydrophilic SO_3H groups the membrane takes up water when exposed to humid environments. The water uptake, expressed as the number of water molecules λ per sulfonic site, increases with relative humidity [2–9]. Phase

* Tel.: +81 80 3396 4286.
E-mail address: dorenbos@ny.thn.ne.jp.

http://dx.doi.org/10.1016/j.jpowsour.2014.07.156
0378-7753/© 2014 Published by Elsevier B.V.

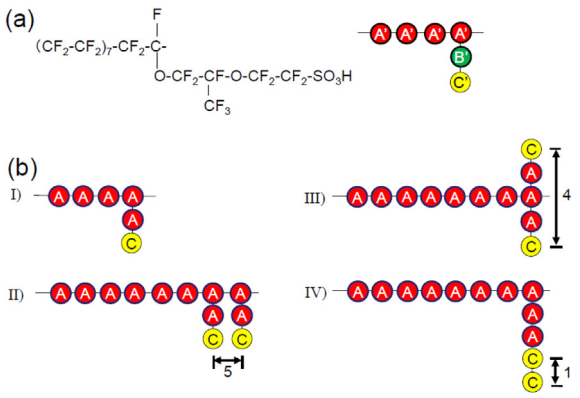

Fig. 1. (a) Repeat unit of Nafion®(EW = 1143) and DPD parameterization as proposed in Ref. 42. A′: CF_2–CF_2–CF_2–CF_2, B′: O–CF_2–CF(CF_3)–O, C′: CF_2–CF_2–SO_3H. (b) Repeat unit of the polymer types. Side chains are branching off from every 4th (I) or 8th (III, IV) A bead along the backbone. For type II side chain branching occurs at every 7th and 8th backbone A bead. The number of bonds or topological distance $D_{topol,1}$ between nearest C beads are given for types II, III, and IV.

separation results in a network with water containing pores a few nm in diameter surrounded by polymer phase [7–9]. Because the pores provide the pathways for water and proton diffusion, the degree of pore connectivity is important to obtain high proton conductivities. At low humidity the proton conductivity decreases rapidly [2–5,7,10,11], which requires a fuel cell design strategy that provides sufficient hydration of the PFSA membranes during operating conditions.

Much effort is spent on the development of new polymers with high proton conductivity. These alternatives have acidic sites located within the backbones of the block polymers or within the side chains of the grafted polymers, such as block polymer type poly-benzimidazole [12], sulfonated poly-ether-ether-ketone [13,14], sulfonated styrene/ethylene-butylene/styrene [10] sulfonated poly aryl ether ketone [15] and bi-phenyl sulfone [16], sulfonated polyimide [17,18], and the grafted [bis] (perfluoroalkyl) sulfonyl imide perfluorinated ionomer [19]. As for the PFSA membranes the presence of hydrophilic acidic sites cause membranes composed of these alternative polymers to swell and phase separate with water uptake.

The amount of water uptake and pore connectivity depends on many parameters such as molecular architecture, side chain distribution and side chain length (grafted polymers), acidic site density, backbone and/or side chain stiffness, and molecular weight. Molecular dynamics (MD) [18–31], coarse grained MD (CGMD) [32,33] and meso-scale approaches such as dissipative particle dynamics (DPD) [34–42] can provide insight in how pore size and pore connectivity are affected by these parameters. MD has been applied frequently to model phase separation within PSFA membranes [18,20–31]. These studies predict water clustering in agreement with experiment. Water and/or proton diffusion constants can be obtained from the mean squared displacements (MSD) of these species. The period over which sampling is performed in MD is typically a few ns which is too small to probe a representative pore network within real membranes. That would require a meso scale simulation in which the system size is significantly larger than the characteristic distance (eg. inter cluster distance) of the pore network. Since within PFSA membranes the characteristic distance is around 5 nm [8,9,11] obstructions in the diffusion pathways can be probed only for system volumes of O(10^4 nm^3) or more.

For system size of ~60 nm^3 Devanathan et al. [27] studied with MD water and proton diffusion through Nafion1143 (1143 is the equivalent weight (EW) of 1143 g polymer/mol SO_3H). A significant increase in diffusion occurred near $\lambda = 5$. For three times larger system size Cui et al. [28] also observed increased water and proton diffusion within Nafion with water uptake, in accordance with experiment. For a volume of ~400 nm^3 Karo et al.[29] [29] simulated water diffusion within Dow (whose side chains are composed of O–CF_2–CF_2–SO_3H) and Nafion at $\lambda = 15$. They noted that the pore morphology depends strongly on system size and questioned conclusions [30] obtained from smaller system size. An MD study by Knox and Voth[31] of Nafion that contained ~20 vol% water involved 2×10^6 atoms (~27000 nm^3). Since the evolvement from a random configuration to an equilibrium structure is impossible for such large system, they pre-assumed 5 different morphologies and a random morphology. With exception of the random morphology, each of them evolved such that the characteristic scattering peak could be reproduced. Therefore solely based on the Bragg reflection peak position in scattering experiments no unique model can be assigned to the specific pore morphology within Nafion.

The effect of side chain distribution on morphology and diffusion was studied by Jang et al. [32] by CGMD. They found less pronounced phase separation and narrower pores for Nafion polymers with uniform side chain attachment as compared to polymers with all side chains located at one end of the backbone. However, water and proton diffusion was not drastically affected by these differences in sequence design. Allahyarov et al. [33] concluded from CGMD simulations that for PFSA like polymers with similar EW those with the longer side chains form larger clusters and higher proton conductivities. This is consistent with DPD studies [35,38] obtained for larger system size.

Dorenbos et al. combined DPD with Monte Carlo (MC) tracer diffusion calculations to predict the dependency of water diffusion on hydration level [34], EW [34,35], side chain length [34,35,38] and Nafion layer thickness (<10 nm) on substrates of various hydrophobicity [36]. The main idea behind the DPD-MC strategy is twofold. Firstly, much larger equilibrium morphologies can be obtained by DPD as compared to MD with minimal computational effort. Secondly, water diffusion can be simulated separately by performing MC tracer diffusion through selected (frozen or static) DPD morphologies. The fast evolvement towards equilibrium morphologies is caused by the soft repulsive interaction that acts between atomic groups that are coarse grained into beads. Therefore topological violations, due to bond crossings, can lift up entanglements in conventional DPD, which explains the absence of polymer reptation motions (D~$1/N^2$, with N number of polymeric backbone beads) [43]. Polymer chains diffuse thus much faster than in an MD simulation.

Due to the polymer bead motion the pore network evolves while water is moving through it. This results in higher water bead motion through the dynamic networks as compared to diffusion through a pore network in which polymer motions are restricted by entanglements. This might in a DPD simulation obscure the dependency of solvent (water) diffusion on various design parameters. Within the DPD-MC scheme this problem is circumvented by mapping the equilibrium-like DPD configurations on a grid and performing MC trajectory calculations through the mapped pore networks. In a recent study [41] it was verified that within hydrated amphiphilic block polymers diffusion constants derived from the water bead motions were indeed higher than MC derived water diffusion constants.

Water diffusion constants within Nafion derived from DPD-MC calculations, in which water diffusion is restricted to the hydrophilic phase that contain both water and sulfuric acid sites, approach experimental diffusion values [34]. More generally it was

predicted that for architectures with same side chain lengths an increase in EW results in increased water cluster size and distance between them but with slower (water) diffusion [34,38]. Theoretical studies on PFSA-like polymers in which also side chain lengths were varied [34,35,38] predicted that at fixed water volume fraction, ϕ_w, for architectures of the same EW those that contain the longer side chains exhibit the largest water clusters, largest inter cluster spacing and fastest diffusion. For the longer side chain architectures also lower percolation thresholds are expected than those containing short side chains [38]. This is caused by different topological distance between nearby hydrophilic sites within the architectures. Architectures with larger topological distance allow the formation of larger and better connected pores, higher diffusion constants at fixed ϕ_w, and lower percolation thresholds. A modified kinetic Monte Carlo based DPD-MC algorithm was developed to study gas diffusion through membranes in which gaseous species have access to both polymer and water phases. This permits to predict the dependence of O_2 and H_2 gas permeability through hydrated Nafion on the membranes' EW [37] within a two phase model.

In the DPD studies addressed above side chains were uniformly grafted along the polymer backbones. Recently it was predicted that for PFSA-like ionomers of the same EW a non-uniform side chain distribution results in better connected pores with increased diffusion [39,40] and lower percolation thresholds [40] as compared to uniform side chain attachments. Also the agreement between experimental and calculated O_2 permeability and water diffusion constants through hydrated Nafion improved for the more realistic architectures with statistically distributed side chains [39].

The purpose here is to predict how water diffusion through the pore networks of membranes of the same EW might be affected by location of the side chains along the backbones. Architectures are considered with one or two side chains branching off from a single backbone bead, and side chains can contain one or two hydrophilic sites (Fig. 1(b)). DPD is used to generate pore morphologies at a fixed hydration level of $\phi_w = 0.16$. Diffusion through the pore networks is modeled by employing Monte Carlo (MC) tracer calculations through selected static (or frozen) DPD morphologies. The diffusion of the water beads through the dynamic pore networks is also studied and obtained DPD diffusion constants are compared with the MC derived values.

The outline of this paper is as follows. In *Computational details* the polymer architectures are presented and the DPD parameterization is outlined. In *Results and analysis* pore morphologies and relations between morphology, chain architecture and MC derived diffusion constants are presented. It is found that differences in diffusion are not due to more water being located within the percolating clusters. Diffusion constants derived from the DPD water bead motions are compared with the MC derived diffusion constants. In *Discussion* the limitations of the used computational approaches are addressed.

2. Computational details

2.1. Polymer chain architecture

In DPD several atoms or molecules are grouped into a single bead. Four types of polymers are considered. A single repeat unit of each type is shown in Fig. 1(b) and contains hydrophobic A beads and one or two hydrophilic C beads. For type I, II, and III the side chains are represented by connected [AC] fragments, whilst a side chain for type IV polymer is two times longer and represented by [A2C2]. Side chains are branching off from every 4th (I), 7th and 8th (II), and 8th (III, IV) A bead along the backbone. For type III polymers two side chains are attached to a single A bead. The DPD formulation of the repeat units are: A4[AC] (I), A7[AC]A1[AC] (II), A8[AC][AC] (III), A8[A2C2] (IV). Six architectures are considered, see Table 1. The number of repeat units for each polymer type is 6 (architectures I, IIIb and IVb) or 3 (architectures II, IIIa and IVa). The number of side chains per polymer is thus $N_{side} = 3$, 6, or 12. This choice results for architectures I, II, IIIa, and IVa in the same polymer length, ie. identical number of backbone beads ($N_{backbone}$) per polymer with $N_{backbone} = 24$. The side chain density, ρ_{side}, expressed as the ratio of the number of side chains and backbone beads, for type I, II, and III are the same with $\rho_{side} = N_{side}N_{backbone}^{-1} = 1/4$ (see Table 1). For type IV ρ_{side} is half this value. Also the two times longer architecture IVb is considered with the same number of side chains as type I, II, and IIIa. For architecture IVb $N_{backbone} = 48$, for this reason also architecture IIIb is included with $N_{backbone} = 48$ and $N_{side} = 12$. The main purpose is to draw trends from architectures for which the lengths are the same (I, II, IIIa, and IVa). Architectures IIIb and IVb are included to verify whether the same trends are observed as between IIIa and IVa for increased polymer length.

Water is represented by W beads. Within the DPD framework followed here (see next paragraph) the volume of each (A, C and W) bead is the same and equal to 0.12 nm^3 which corresponds to the volume occupied by 4 water molecules. The (dry) acidic site densities are thus 2.31 $mmol/cm^3$. The ion exchange capacity (IEC) expressed in mmol/gr can be obtained when the mass densities of the molecular fragments are known. For instance, for a polymer with a mass density of 1 gr/cm^3 the IEC would be 2.31 mmol/gr (or EW of 433 gr/mol).

2.2. Dissipative particle dynamics

Hoogerbrugge and Koelman [44] introduced DPD to study hydrodynamics. DPD is used in modeling eg. phase separation [45], membrane rupture [46], vesicles [47,48] and drug delivery [49]. Here the framework developed by Groot and Warren [50] is followed which can be considered as standard and therefore the most essential details are given here. According to Newton's equations of motion beads evolve as: $d\boldsymbol{r}_i/dt = \boldsymbol{v}_i$, $m_i d\boldsymbol{v}_i/dt = f_i$, with m_i, $\boldsymbol{r}_i$ and $\boldsymbol{v}_i$, the mass, position and velocity of bead i. Interactions between beads i and j are given by conservative F_{ij}^C, dissipative F_{ij}^D, and random F_{ij}^R forces. The force f_i acting on bead i is given by Eq. (1).

$$f_i = \sum_{j \neq i} F_{ij}^C + F_{ij}^R + F_{ij}^D \tag{1}$$

The sum is over all particles j located within a cutoff distance r_c that defines the length scale. F_{ij}^C is soft repulsive and decreases linearly with distance between beads:

$$F_{ij}^C = \begin{cases} a_{ij}\left(1 - \dfrac{r_{ij}}{r_c}\right)\hat{\mathbf{r}}_{ij} & (r_{ij} < r_c) \\ 0 & (r_{ij} \geq r_c) \end{cases} \tag{2a}$$

Table 1
Number of side chains (2nd column), backbone beads (3rd column) and side chain density (4th column) for each architecture. The topological distance $D_{topol,1}$ (5th column) and $D_{topol,2}$, (6th column) are the number of bonds between nearest and next nearest C beads within the architectures, respectively. 7th column: Total number of polymers, N_{pol} in simulation box.

Architecture	N_{side}	$N_{backbone}$	ρ_{side}	$D_{topol,1}$	$D_{topol,2}$	N_{pol}
I: A4[AC]-6	6	24	4^{-1}	8	8	968
II: A7[AC]A1[AC]-3	6	24	4^{-1}	5	11	968
IIIa: A8[AC][AC]-3	6	24	4^{-1}	4	12	968
IIIb: A8[AC][AC]-6	12	48	4^{-1}	4	12	484
IVa: A8[A2C2]-3	3	24	8^{-1}	1	14	968
IVb: A8[A2C2]-6	6	48	8^{-1}	1	14	484

$$\mathbf{r}_{ij} = \mathbf{r}_i - \mathbf{r}_j, \quad r_{ij} = |\mathbf{r}_{ij}|, \quad \hat{\mathbf{r}}_{ij} = \mathbf{r}_{ij}/|\mathbf{r}_{ij}| \tag{2b}$$

In Eq. (2) $\hat{r}_{ij}$ is the unit vector in the direction of bead j towards bead i: F_{ij}^R corresponds to thermal noise (Eq. (3)), and F_{ij}^D is proportional to the beads' relative velocity (Eq. (4)).

$$F_{ij}^R = \sigma\omega^R(r_{ij})\zeta_{ij}(\Delta t)^{-0.5}(k_BT)^{-1}\hat{r}_{ij} \tag{3}$$

$$F_{ij}^D = -\gamma\omega^D(r_{ij})(\hat{r}_{ij}\cdot\mathbf{v}_{ij})\hat{r}_{ij} \tag{4}$$

$\mathbf{v}_{ij} = \mathbf{v}_i - \mathbf{v}_j$, ω^D and ω^R are weight functions, ζ_{ij} introduces randomness into the system involving a randomly fluctuating variable with Gaussian statistics with zero mean and unit variance: $<\zeta_{ij}(t) \geq 0$, and $<\zeta_{ij}(t)\zeta_{kl}(t') \geq (\delta_{ik}\delta_{jl} + \delta_{il}\delta_{jk})\delta(t-t')$. For each pair of beads there is an independent random function. ω^D and ω^R are given by Eq. (5).

$$\omega^D(r_{ij}) = \left[\omega^R(r_{ij})\right]^2 = \begin{cases} \left(1 - \dfrac{r_{ij}}{r_c}\right)^2 & (r_{ij} < r_c) \\ 0 & (r_{ij} \geq r_c) \end{cases} \tag{5}$$

Noise (σ) and friction (γ) parameters are related as $\sigma^2 = 2\gamma k_BT$ [51] with $\sigma = 3$, $\gamma = 4.5$, k_B the Boltzmann constant and T the temperature. All three forces act along the line of centers and conserve linear and angular momentum. Adjacent beads that belong to the same polymer are joined by a spring force with spring constant $C = 50$ and equilibrium bond distance $R_0 = 0.85\ r_c$:

$$F_{ij}^S = -C(r_{ij} - R_0)\hat{\mathbf{r}}_{ij} \tag{6}$$

As for the interaction range r_c, the mass of all beads and the unit of energy (k_BT) are scaled to 1. The unit of time $\tau = r_c\,(m/k_BT)^{0.5}$ is also equal to 1. The temperature is kept constant near $k_BT = 1.0$ by solving the equations of motion using a modified Verlet integration scheme [50] with empirical factor 0.65 and time step $\Delta t = 0.05$. The bead density ρ is 3.

The repulsions a_{ij} are listed in Table 2. Those between incompatible (hydrophobic *vs* hydrophilic) beads are highest (A–W and A–C). Repulsions between similar beads are set at 104 which reproduces water compressibility [34,39,42]. The other repulsions are calculated from the Flory-Huggins χ parameters (Table 2) that are comparable with those derived from calculated binding energies for the molecular fragments of Nafion by Yamamoto and Hyodo [42]. They parameterized a Nafion repeat unit as A′4[B′C′] (Fig. 1(a)) with hydrophobic A′ (CF_2–CF_2–CF_2–CF_2) and B′ (O–CF_2–CF–CF_3–O) beads and hydrophilic C′ (CF_2–CF_2–SO_3H) beads, and obtained $\chi_{A'W} = 5.79$, $\chi_{B'W} = 4.9$, $\chi_{C'W} = -2.79$, $\chi_{A'B'} = 0.02$, $\chi_{A'C'} = 3.11$. Here polymers are constructed of hydrophobic A and hydrophilic C beads (Fig. 1(b)). The χ parameters between hydrophobic and hydrophilic (C and W) beads are chosen to be $\chi_{AC} = \chi_{AW} = 4.9$. This value is equal to $\chi_{B'W} = 4.9$ [42] and between $\chi_{A'W} = 5.79$ and $\chi_{A'C'} = 3.11$. $\chi_{CW} = -2.6$ is close to $\chi_{C'W} = -2.79$ estimated in Ref. [42].

The χ-values in Table 2 were adapted in previous works [38–41] and resulted in well phase separated morphologies. They are also expected to result in phase separated morphologies for the current architectures. For the sake of generality, atomistic calculations to obtain χ parameters for given chemical formulae of the beads were omitted. Important is the incompatibility between A and C beads, with (A)C fragments (un)favorably interacting with water. The χ parameters in Table 2 were also used in earlier modeling of phase separation within amphiphilic block and amphiphilic grafted polymers. Therefore an already existing database is extended in this work.

Table 2
DPD repulsions and χ_{ij}-parameters (parenthesis).

	A	C	W
A	104 (0)		
C	124.4 (4.9)	104 (0)	
W	124.4 (4.9)	93.2 (−2.6)	104 (0)

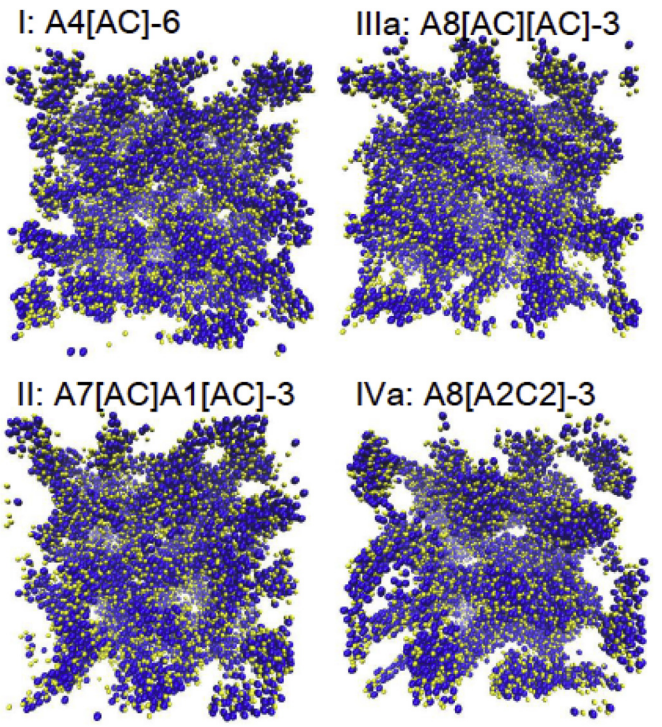

Fig. 2. Snapshots of pore morphologies obtained at $2 \times 10^4\Delta$t for four membrane types (C beads: yellow (light grey), W beads: blue (dark)). (For interpretation of the references to color in this figure legend, the reader is referred to the web version of this article.)

The DPD repulsions that correspond with the χ-parameters are obtained from Eq. (7) [41].

$$\Delta a_{ij} = (4.16\pm0.15) \times \chi_{ij} \tag{7}$$

The water volume fraction ϕ_w is given by Eq. (8), with N^A, N^W and N^C the total number of A, W and C beads.

$$\phi_w = \frac{N^W}{N^W + N^A + N^C} \tag{8}$$

In this work $\phi_w = 0.16$. Since each W bead represents 4 water molecules, the water content expressed in terms of λ is given by Eq. (9).

$$\lambda = \frac{N^W}{N^C} \times 4 \tag{9}$$

For $\phi_w = 0.16$ the corresponding λ value is 4.6.

The system is cubic with cell dimension of $L = 24$. One DPD length unit corresponds to $r_c = (3 \times 0.12)^{1/3}$ nm^3 = 0.71 nm. Box edge lengths are $L \times r_c$ ~17 nm and volumes are ~5×10^3 nm^3. The simulation box contains 41472 ($=\rho \times L^3$) beads (6624 W beads and $N_{pol} = 968$ or 484 polymer chains). Periodic boundaries are applied in the orthogonal directions. The physical time to which τ corresponds for $a_{ww} = 104$ is ~130 ps. Morphologies were generated up

to 4×10^4 Δt and correspond with a duration of O (0.2 μs). Figures that display morphologies were generated using the VMD-visual molecular dynamics package [52].

3. Results and analysis

3.1. Pore morphology

In Fig. 2 snapshots of morphologies obtained at $t = 2 \times 10^4$ Δt are displayed. Only C and W beads are shown. For all morphologies, C beads are associated with W beads and form a hydrophilic (C + W) pore network. For architecture I the pores appear to be most dispersed, with narrow connections between the clusters. For architecture III the pores are most well developed and cylindrically shaped. The water clusters are largest, less dispersed and most spherical for architecture IV. From visual inspection of the morphologies during a DPD run it was observed that the pore networks are capable to slightly change their morphology. This is illustrated for the A8[AC][AC]-3 architecture in Fig. 3, where snapshots taken at intervals of 4000Δt (or 200τ) are displayed (for instance by comparison of the morphology obtained at $t = 12000\Delta t$ with that at $t = 32000\Delta t$).

The extent of morphological variation during the DPD runs was also examined by inspection of the W-bead pair correlation functions, g(r). Examples of the time evolution of g(r) are given in Fig. 4(a)–(d). The average distance between water clusters, $D_{\text{Cl-Cl}}$, can be estimated from the position of the second maximum [34,42] (located between 4 nm and 7 nm). $D_{\text{Cl-Cl}}$ is plotted against DPD time in Fig. 5(a). After an initial increase $D_{\text{Cl-Cl}}$ tends to stabilize beyond ~$10^4\Delta t$. The $D_{\text{Cl-Cl}}$ values that were averaged over the period $2 \times 10^4\Delta t – 4 \times 10^4\Delta t$ for all six architectures are listed in Table 3.

In Fig. 5(b) the increase in $D_{\text{Cl–Cl}}$ with respect to architecture I (A4[AC]-6), is plotted against $D_{\text{topol,2}}$-$D_{\text{topol,1}}$, where $D_{\text{topol,1}}$ is defined as the smallest possible topological distance between two nearest C beads (in units of number of bonds or springs, see Fig. 1(b)), and $D_{\text{topol,2}}$ is the smallest possible distance between a C bead and its 2nd nearest C bead. $\Delta D_{\text{Cl–Cl}}$ increases non-linearly with $D_{\text{topol,2}}$-$D_{\text{topol,1}}$. These results are in line with studies [39] in which a quadratic dependency was found for in total 18 Ax[AC]Ay[AC] architectures of several IEC with various values of x and y. In Ref. 39 the bead volumes were half the size of those in this work with diagonal repulsions of $a_{\text{ww}} = 51$ but with chi parameters being the same as here.

3.2. MC tracer diffusion through static pore networks

The pore connectivity can be probed by MC trajectory calculations by restricting the tracer particle movement to the pore phase [34]. By following the random movement of the particles, tracer diffusion coefficients can be determined. The particle movement takes place on a cubic grid of size 240^3 (1.4×10^7 nodes). On this grid the W pore network is constructed such that nodes for which the nearest bead is a W bead belong to the pore phase. After construction of the pore network 2000 particles ($N_{\text{tracer}} = 2000$) are initially put at randomly selected nodes that belong to the pore phase. During every Monte Carlo step (MCS), a jump trial towards a nearest node in one of the six orthogonal directions is randomly selected for each particle independently. A trial is successful when the aimed site belongs to the W (or pore) phase. Diffusion constants are obtained from the MSD of N_{tracer} trajectories (Eq. (10)):

$$D = \frac{1}{6N_{\text{tracer}}} \lim_{t\to\infty} \frac{\mathrm{d}}{\mathrm{dt}} \sum_{i=1}^{N} \left\langle \left[R_i(t) - R_i\left(t'\right) \right]^2 \right\rangle \tag{10}$$

MSD curves obtained for morphologies generated at $t = 4 \times 10^4\Delta t$ are displayed in Fig. 6(a). Also the pure water case, for which every jump trial is accepted and the slope is per definition equal to 1, is displayed in Fig. 6(a). Diffusion constants within the membranes, D_{MC}, can be expressed relative to that of pure water according to Eq. (11) [34,38–41].

$$D_{\text{MC}} = \frac{\Delta(MSD)}{\Delta(MCS)} \tag{11}$$

The Δ(MSD)/Δ(MCS) slopes were determined by linear fitting over the time window $3 \times 10^5 – 6 \times 10^5$ MCS.

Fig. 6(b) displays D_{MC} values against DPD time. No persistent increasing or decreasing trend of D_{MC} with DPD time is observed beyond $2 \times 10^4\Delta t$. This indicates that equilibration has been reached, and is in accordance with conclusions derived from g(r), where $D_{\text{Cl–Cl}}$ was found to stabilize beyond ~$10^4\Delta t$ (Fig. 5(a)). Despite the apparent convergence of D_{MC} and g(r), D_{MC} values are

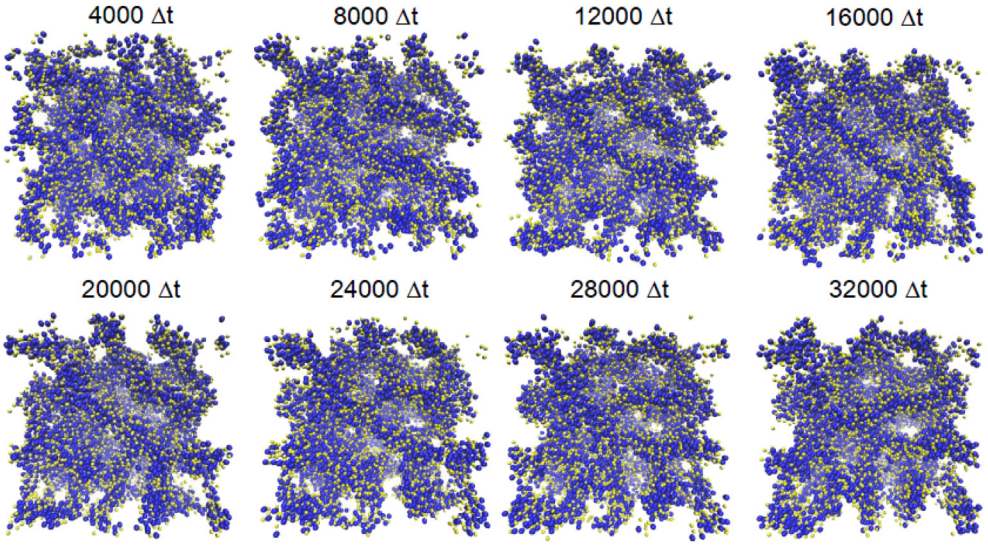

Fig. 3. Example of time evolution of the pore network for A8[AC][AC]-3 architecture. C beads are colored yellow (light grey) and W beads are blue (dark). (For interpretation of the references to color in this figure legend, the reader is referred to the web version of this article.)

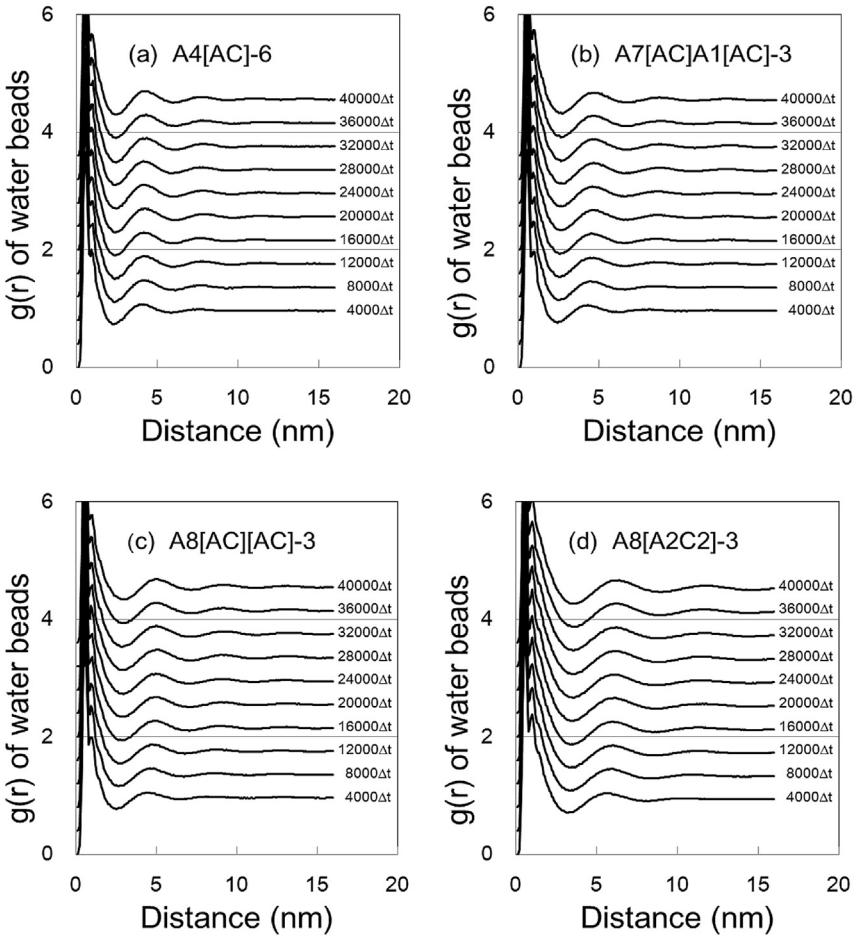

Fig. 4. Time evolution of W bead pair correlation functions obtained for membranes of type I: A4[AC]-6 (a), II: A7[AC][A1[AC]-3 (b), III: A8[AC][AC]-3 (c) and IV: A8[A2C2]-3 (d). For increasing time the curves are shifted upwards with a constant along the vertical axes.

fluctuating which indicates that the morphologies are continuously changing, and connections between pores might become better (resulting in enhanced D_{MC}) or worse. Diffusion constants through the frozen morphologies averaged over the time window $2 \times 10^4\Delta$dt–$4 \times 10^4\Delta t$ are listed in Table 3 and are plotted against D_{Cl-Cl} in Fig. 7. For polymers with one C bead (type I, II, III) within each side chain, D_{MC} increases with D_{Cl-Cl}. For type IV polymer, which contains 2C beads per side chain this is also the case with D_{Cl-Cl} being substantially larger.

For polymers of similar length with $N_{backbone} = 24$, diffusion turns out to be highest for architecture III. For the longer IIIb and IVb ($N_{backbone} = 48$) architectures water diffusion is lower than for IIIa and IVa, respectively (Fig. 7). D_{Cl-Cl} is also lower for the longer architectures. MC diffusion constants were obtained from frozen lattices, therefore differences in diffusion are caused by differences in pore morphologies. Apparently the longer architectures tend to be less capable to provide good connected large pores, because more C beads are restricted to be attached to the same polymer.

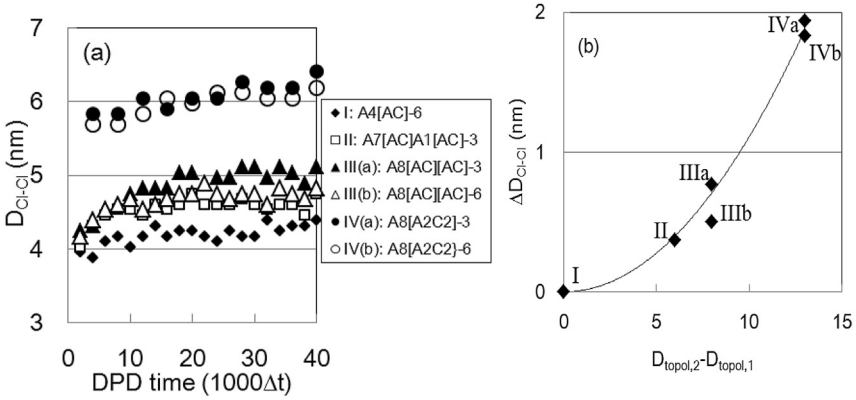

Fig. 5. (a) D_{Cl-Cl} plotted against DPD time for all six architectures. (b) Increase in D_{Cl-Cl} ($\Delta D_{Cl-Cl} = D_{Cl-Cl} - D_{Cl-Cl}$(A4[AC]-6)) plotted against difference in topological distance between 2nd nearest ($D_{topol,2}$) and nearest ($D_{topol,1}$) C beads within the architectures. Values of ΔD_{Cl-Cl} are averages over time window $2 \times 10^4\Delta$t–$4 \times 10^4\Delta$t. The drawn curve is a quadratic function (y = constant$\times x^2$).

Table 3
Average distance between water clusters D_{Cl-Cl} and diffusion constants D_{MC} derived from MC tracer simulations.

Architecture	D_{Cl-Cl}	D_{MC}
I: A4[AC]-6	4.25 nm	0.048
II: A7[AC]A1[AC]-3	4.62 nm	0.085
IIIa: A8[AC][AC]-3	5.02 nm	0.131
IIIb: A8[AC][AC]-6	4.75 nm	0.108
IVa: A8[A2C2]-3	6.19 nm	0.103
IVb: A8[A2C2]-6	6.08 nm	0.089

I conclude with the following remarks: (i) For all architectures D_{Cl-Cl} increases with $D_{topol,2}$- $D_{topol,1}$ (Fig. 5(b)); (ii) For both [AC] and [A2C2] type architecture D_{MC} increases with D_{Cl-Cl} (Fig. 7); (iii) For architectures (I, II, IIIa and IVa) which are of the same length with $N_{backbone} = 24$ diffusion is highest for type III architecture. Among the architectures for which $N_{backbone} = 48$ (IIIb and IVb) also type III reveals the highest diffusion.

3.3. Largest connected water cluster

Whether variations in D_{MC} are due to differences in the amount of water being located within isolated clusters, or whether diffusion is to various extent limited by the presence of narrow connections within the percolating water cluster was verified by calculating the cluster size distribution (CSD) of the W beads. Here, a water cluster is defined to be of size N^{cl} when it contains N^{cl} W beads and the distance of each W bead within that cluster to at least one of the remaining N^{cl}-1 beads within that cluster is less than L_{bond}. Due to the repulsive interactions between DPD beads (Eq. (2)) W beads are not randomly distributed within the water phase. For very small L_{bond} values W beads can thus not be contained within large clusters and each W bead will be isolated. But for L_{bond} values near or well above the first peak in the pair correlation function (Fig. 4) water clustering occurs.

Since the first peak in the pair correlation function is located near $0.85r_c$ W clustering is expected for L_{bond} near or above $0.85r_c$. This was verified by calculating the CSD as function of L_{bond} from the positions of W beads for an equilibrated DPD system that contained only W beads. The size of the largest W cluster was found to increase sharply beyond $L_{bond} = 0.8$, and for $L_{bond} = 0.85$ more than 99.9% of the total number of W beads was contained in one cluster. For all morphologies the largest W cluster was obtained from the CSD calculated for $L_{bond} = 0.85$ and $L_{bond} = 0.9$. The results for $L_{bond} = 0.85$ are plotted against DPD time in Fig. 8. Beyond $10^4\Delta t$ it is found that with exception of architecture I (A4[AC]-6) a vast majority of the total amount of W beads is located within a single cluster. The largest cluster for architecture I contains between 20% and 40% of the total amount of W beads for $L_{bond} = 0.85$ (Fig. 8). For $L_{bond} = 0.9$ between 70% and 90% of the total number of W beads were found to join one cluster for $t > 4 \times 10^3\Delta t$. The variations in D_{MC} observed for architectures II, III and IV (Table 1) are thus not due to differences in percolating cluster size but due to more salient differences within the internal structure of the percolating network (bottlenecks, dead ends etc.).

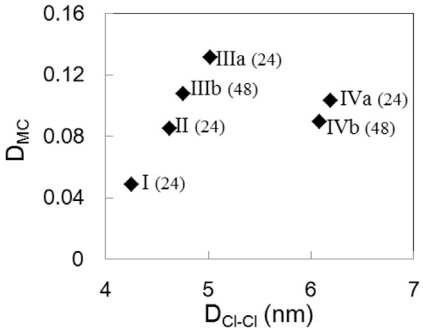

Fig. 7. Tracer diffusion coefficients D_{MC} vs inter cluster distance D_{Cl-Cl} obtained for the architectures listed in Table 1.The backbone lengths are given in parenthesis.

3.4. DPD W bead diffusion through dynamic pore networks

Diffusion coefficients can in principle also be calculated from the ensemble average, $D^{Membrane}_{W-bead}$, of the MSD of W beads during the DPD simulations. The molecular water diffusion coefficient within the membrane $D^{Membrane}_{H_2O}$ is then obtained by comparing $D^{Membrane}_{W-bead}$ with the W bead diffusion coefficient $D^{Pure\ water}_{W-bead}$ for a system solely composed of W beads according to Eq. (12a), with $D^{Pure water}_{H_2O}$ the pure water diffusion coefficient of 2.3×10^{-5} cm^2 s^{-1}.

$$D^{Membrane}_{H_2O} = \frac{D^{Membrane}_{W-bead}}{D^{Pure\ water}_{W-Bead}} \times D^{Pure\ water}_{H_2O} \quad (12a)$$

$$D_{DPD} = \frac{D^{Membrane}_{W-bead}}{D^{Pure\ water}_{W-Bead}} \quad (12b)$$

Instead of deriving diffusion coefficients from the DPD W bead movements the MC approach was applied in Section 3.2. One of the

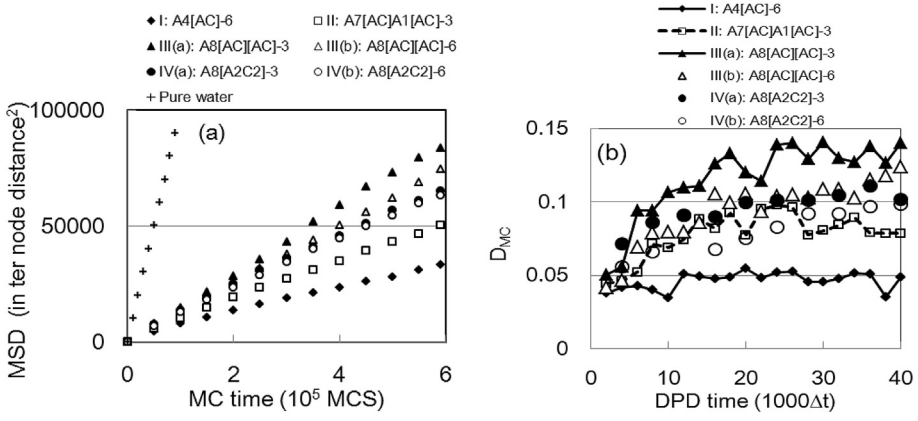

Fig. 6. (a) Examples of MSD curves within the DPD pore networks ($t = 4 \times 10^4\Delta t$) for architectures I, II, IIIa, IIIb, IVa and IVb. The pure water case ($\phi_w = 1.0$), for which the slope is equal to 1, is included (crosses). (b) D_{MC} plotted against DPD time.

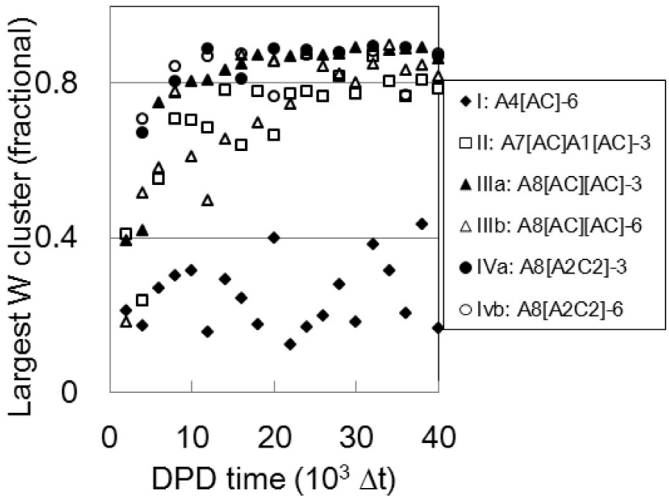

Fig. 8. Time evolution of size of largest water cluster for all six architectures, $L_{bond} = 0.85$.

reasons was that DPD allows bond crossings that lift up entanglements. This causes DPD polymers to diffuse faster than real polymers, resulting in fast evolvement to equilibrium like morphologies. As a result, the DPD pore morphology may change while the water beads are diffusing through it. For this reason, frozen (static) DPD morphologies were taken as input for the MC trajectory calculations and the pore networks were thus fixed in time.

Since the pores can rearrange continuously the relative W bead diffusivities, D_{DPD} (defined by Eq. (12b)), expressed relative to pure water diffusion are expected to be higher than the D_{MC} values. The D_{DPD} values are compared with D_{MC} in Fig. 9(a) (filled symbols). D_{MC} and D_{DPD} are highest for type III architectures and lowest for architecture I. As expected, the D_{DPD} diffusivities differ from the MC derived diffusivities with D_{DPD} being between a factor 2.5 and 4.3 higher than the D_{MC} values.

C beads are the end moieties of the pendant side chains (Fig. 1(b)) and are located near the W pore network (Fig. 2). Their pendant motion (and A bead motions as well) result in a continuous rearrangement of the W pore network (Fig. 3). Now naively assume that the A beads are fixed in space for $t > 20000\Delta t$. The W beads can then have access to at most the whole hydrophilic phase which constitutes a volume fraction of 0.30 ($\phi_{W+C} = \phi_W + \phi_C = 0.3$). Additional MC trajectory calculations were repeated within the mapped DPD morphologies sampled at $t > 20000\Delta t$ in which tracer particles can diffuse freely through the mapped hydrophilic (W + C) networks. D_{DPD} is plotted against thus calculated MC diffusion constants, D_{MC}(W + C) in Fig. 9(b). D_{DPD} is systematically higher than D_{MC}(W + C). W beads are thus more mobile than expected for a fixed C + W pore network. Apparently the mobility of the A beads also causes increase of W bead diffusion due to the spatiotemporal evolvement of the pore networks.

During a DPD simulation the C + W pore network can be made nearly static by increase of the polymer A bead masses which is expected to result in a lower W bead mobility. This was verified by rerunning the DPD simulations starting from the configurations shown in Fig. 2 ($t = 2 \times 10^4 \Delta t$). D_{DPD} obtained for $m_{A\text{-bead}} = 1000$ and $m_{C\text{-bead}} = m_{W\text{-bead}} = 1$ are given in Fig. 9(a). Diffusivities of the DPD W beads turn out to be still a factor ~1.3–~1.7 larger than the D_{MC} averages. A further decrease of D_{DPD} is obtained by also increasing the C bead mass. For $m_{A\text{-bead}} = m_{C\text{-bead}} = 1000$ the D_{DPD} values approach those obtained from D_{MC} for architecture I but for the other architectures are less than D_{MC} (Fig. 9(a)). Apparently the decreased mobility of the C beads strongly influences W bead transport through the nearly static pore networks. It is well possible that the low C bead motion for $m_{C\text{-bead}} = 1000$ causes W beads to be caged in and trapped for longer periods resulting in a significant decrease of D_{DPD}.

4. Discussion

The polymer lengths for architectures I, II, IIIa and IVa were the same ($N_{backbone} = 24$). The calculated tracer diffusion constant, D_{MC}, for water diffusing through the frozen W network is largest for architecture IIIa (Fig. 7). When tracer particles are also allowed to move through the W + C network diffusion increases but the trends are not affected with architecture IIIa revealing the highest diffusion constant, D_{MC}(W + C) (Fig. 9(b)). For each architecture D_{MC}(W + C) is only slightly less than the W bead diffusion constant D_{DPD} (Fig. 9(b)), which suggested that W beads diffusing through the "spatiotemporally evolving membrane" can pass through the region previously occupied by a C bead. In the DPD simulations, the polymer motions thus promote W bead transport. This was verified by decreasing the A or (A and C) bead mobility by increasing their masses. This caused a significant lower W bead diffusion which approach the MC values for diffusion through the frozen W networks (Fig. 9(a)).For real membranes a reduction of polymer motion occurs by temperature decrease, which is expected to reduce polymer assisted water diffusion. Hypothetically, the D_{MC} diffusion constants obtained for tracer diffusion through the static DPD pore networks are then lower bounds for low temperature conditions

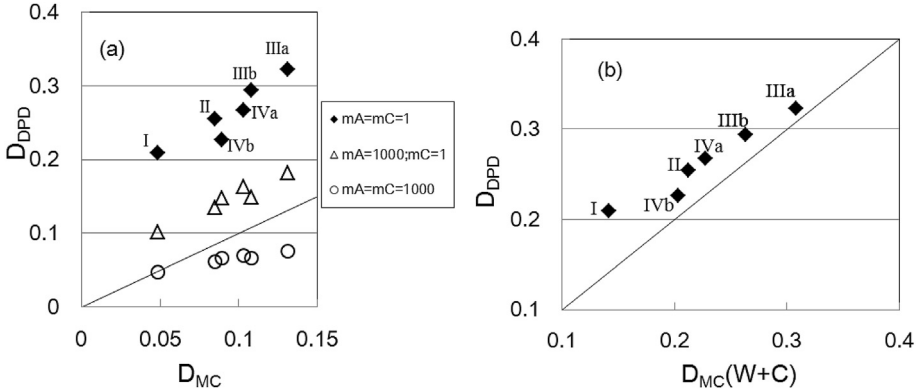

Fig. 9. (a) DPD W bead diffusion constants vs D_{MC} within the static DPD morphologies. Bead masses are equal to 1 (filled diamonds); $m_{A\text{-bead}} = 10^3$ (open triangles); $m_{A\text{-bead}} = m_{C\text{-bead}} = 10^3$ (open circles). (b) D_{DPD} vs D_{MC}(W + C). All bead masses are equal to 1.

(when morphology is not affected and locally water diffusion resembles that of pure water at that lower temperature).

Comparison between the larger polymers IIIb and IVb with $N_{backbone} = 48$, also reveals for type III polymer the highest water diffusion constants, D_{MC} (Figs. 9(a) and 7), $D_{MC}(W + C)$ (Fig. 9(b)) and D_{DPD} (Fig. 9(a)). For the longer IIIb and IVb sequences the W bead diffusion constant D_{DPD} (Fig. 9) is lower than for IIIa and IVa, respectively. Since also within the static morphologies D_{MC} (Fig. 7) and $D_{MC}(W + C)$ (Fig. 9) are lower for the longer architectures, the difference is not attributed to a different extent to which polymer motions assist in W bead diffusion. The decrease in W bead diffusion is thus due to different pore morphologies with lower D_{Cl-Cl} values for the longer (IIIb and IVb) architectures (see Fig. 7). Within real polymer membranes intrinsic backbone stiffness, due to bending constraints along the polymer backbone, may also affect the formation of good connected pores required for fast water diffusion. In the present simulations bending stiffness was not included.

Water diffusion derived from MC simulations through the frozen (W or W + C) networks shows the same trends with respect to polymer architecture as derived from the DPD W bead motions through the evolving pore network (see Fig. 9). Trends are also not affected by decreasing the polymer mobility by selecting higher polymer bead masses. This validates to derive correlations between polymer architecture and water transport in the membrane. This is because water only diffuses through the hydrophilic (W or W + C) phase and in both MC and DPD modeling the local water diffusion constant in the water phase is the same as that of pure water. In modeling water transport, the use of frozen DPD morphologies as input for MC tracer diffusion calculations to predict relations between polymer architecture and water transport is therefore an appropriate approach.

In modeling gas transport more care should be taken into account. Within membranes the gas concentration and mobility depends on the phase in which the gas species resides. Gas permeation cannot be simulated by conventional DPD since it requires the introduction of gas beads that reproduce gas solubility and gas diffusion within polymer and water phase. DPD in combination with (kinetic) MC, however, can reveal trends that relate the EW and water content dependence of O_2 permeability through Nafion [37,39]. These studies rely on the assumption that the gas solubility and diffusion in both phases are the same as in the two pure component phases. O_2 permeation in Nafion has also been proposed to be promoted by polymer flexibility [53] and to occur mainly in the intermediate region located in the polymer matrix near the ionic clusters [53,54]. This cannot be modeled by DPD since it would require the reproduction of the gas solubility and diffusion within three distinct (water, polymer, and intermediate) phases. Also KMC calculation of gas permeation through frozen lattices obtained from DPD requires these six parameters as input. Only when these are known (from experiment or MD simulations) DPD combined with KMC might be value to model gas permeation through meso-scale pore networks.

The interactions between hydrophobic (A) and hydrophilic (C, W) beads were chosen close to those used in previous modeling on Nafion. Therefore it may be expected that membranes composed of PFSA-like polymers of type III (Fig. 1(b)) result in better pore connectivity and higher solvent diffusion constants and proton conductivity as well. As an example, two additional simulations were performed using the χ-parameters proposed for Nafion in Ref. 42 (given in Section 2.2). According to Eq. (7) the DPD repulsions are: $a_{A'B'} = 104.1$; $a_{A'C'} = 116.9$, $a_{A'W} = 128.1$; $a_{B'C} = 109.7$; $a_{B'W} = 124.4$; $a_{C'W} = 92.4$. Using these repulsions the obtained values for D_{MC} at $t = 20000\Delta t$ for A4′[B′C′]-6 and A8′[B′C′][B′C′]-3 at $\phi_w = 0.16$ are 0.014 and 0.122, respectively. For $D_{MC}(W + C)$ respectively 0.064 (A4′[B′C′]-6) and 0.246 (A8′[B′C′][B′C′]-3) are obtained. Diffusion within A8′[B′C′][B′C′] membranes are thus systematically higher than within A4′[B′C′] membranes.

When the $D_{MC}(W + C)$ values are converted to physical diffusion constants $D_{phys}(H_2O)$ then 1.5×10^{-6} cm^2 s^{-1} and 5.5×10^{-6} cm^2 s^{-1} are obtained for the A4′[B′C′]-6 and A8′[B′C′][B′C′]-3 architectures, respectively. For comparison the experimental value for Nafion1100 at $\phi_w = 0.16$ derived from Fig. 4(a) in Ref. 11 is ~2×10^{-6} cm^2 s^{-1}, which is in the same range as derived here.

The above example illustrates that enhanced water diffusion predicted for two side chains branching off from backbones does not only occur for the repulsions used in Table 2 but for a range DPD repulsions. PFSA polymers in a PEFC may contain several hundred side chains [55], and their distribution along the backbone is not precisely known. Also the dependency of water diffusion on polymer length is not known. An exact reproduction of experimental diffusion constants can thus not be expected.

In total 120 pore morphologies that were obtained by DPD for six architectures were subjected to MC tracer diffusion simulations on a lattice. These MC simulations were robust, neglecting any dynamical coupling between water and polymer, and no correlations between the water molecules were assumed. The only assumption was that the local molecular water mobility within the pores is the same as that within pure water. Despite this oversimplification, quasi elastic neutron scattering studies [56,57] on hydrated Nafion membranes indeed concluded that within the nm scale pores the water diffusion constant is close to that of pure water. For instance, Pivovar and Pivovar [57] measured at a water content of ~14 vol% a local water mobility of 1.6×10^{-5} cm^2 s^{-1}, which is only 30% below the pure water diffusion constant of 2.3×10^{-5} cm^2 s^{-1}. Since the obtained MC tracer diffusion constants within the (W or W + C) pores correlate strongly with the DPD W bead diffusion constant, it is obvious that it is the pore topology that mostly affects the diffusion of water beads (molecules).

Flexible polymer backbones and side chains were assumed (no bending constraints). This allowed the relaxation towards morphologies with optimized compatible (W–W, C–W, A–A) contacts and minimized number of incompatible hydrophobic–hydrophilic (A–W, A–C) contacts. Backbone chain lengths as reported for realistic PFSA polymers [55] are at least one order of magnitude larger than here. Further improvement of diffusion might be to see if there is for each architecture type an optimal polymer length which results in highest water diffusion. For the sake of a fair comparison, the polymer backbone lengths for architectures I, II, IIIa, and IVa were intentionally kept fixed at $N_{backbone} = 24$. But a dependency on polymer length was found when comparing architecture IIIa, IVa vs. IIIb, IVb ($N_{backbone} = 48$). The effect of intrinsic chain stiffness, not considered here, may affect the pore morphology and water diffusion. For fixed chain stiffness an optimum in chain length might be present to facilitate water (cq. proton) diffusion. Also adjusting χ parameters might optimize diffusion. For block polymers also a χ-parameter dependency on diffusion was found [35]. Fine tuning by searching for optimized polymer lengths, χ-parameters, or bending stiffness was not the intention of this work, but worthwhile to look for in future studies.

For realistic membranes that are applied in a PEFC, some rigidity is necessary. The rigidity is partly obtained by the presence of micro crystals [11]. DPD does not permit to study polymer crystallization. Therefore the extent to which crystallization impairs the formation of the optimized morphologies could not be studied here. It is well possible that the amount of crystallization is higher for architectures with side chains separated far apart along the polymer backbone. In the present study these are the architectures of type III (A8[AC][AC]) and IV (A8[A2C2]) for which also the largest D_{Cl-Cl}

were obtained (Fig. 7). Interestingly, the larger hydrophobic space between the clusters for these architectures as compared to A4[AC] architectures might favor the formation of small polymeric crystals necessary for the required rigidity.

Electrostatic interactions were not explicitly taken into account in the DPD simulations. Therefore the phase separated morphologies in this work are a consequence of both bead connectivity (chain architecture) and the choice of χ parameters. It would be interesting to see to what extent the results are affected when electrostatic interactions are explicitly taken into account. From earlier DPD studies [39,40] it was found that C beads which are topologically close together within a certain architecture (low $D_{to\text{-}pol,1}$ value) tend to join the same pore or water cluster. For C beads that are close to each other, the electrostatic interactions between them are also expected to affect the distance between them. For low hydration levels the C beads have a neutral character. With increasing hydration proton dissociation occurs, which leaves the protons in the water clusters. This may result in repulsion between nearby C beads with increase in hydration level. These issues were beyond the scope of this work and should be challenged by ab initio or MD methods. Noteworthy is that a total reflectance infrared spectroscopy study [58] revealed that for Nafion the sulfonic site is protonated at dry and dissociated in hydrated Nafion. Combined with ab initio calculations Webber et al. [58] found that sulfonic acid sites are deprotonated above a hydration level of $\lambda = 4$, in accordance with other ab initio work on Nafion or Dow membranes [59].

One of the main conclusions is that the simulations presented in this work predict that ionomers composed of A8[AC][AC] and A′8[B′C′][B′C′] repeat units give rise to faster water diffusion, or better connected pore networks, as compared to those composed of A4[AC] and A′4[B′C′] repeat units, respectively. To my knowledge, at present it is difficult to validate this prediction experimentally since precise control of branching distribution is not feasible during polymer synthesis.

Finally, it would be worthwhile to perform a fine graining of the present work for system size of O(10^4 nm^3) by MD simulations for the architectures in Fig. 1(b). As mentioned in the Introduction the evolvement from pre-assumed morphologies [31] can then be studied for such system size. After fine graining the equilibrium-like DPD morphologies, they can then serve as starting morphologies to study their stability and evolvement. Also the evolvement from random configurations toward equilibrium structures might be studied by MD. By repeatedly creating periodic images that are again equilibrated large scale structures can then be obtained [60]. Support for the findings here can then be obtained when a comparison is made between the molecular water diffusion constants and that of W beads through the DPD morphologies for the architectures in Fig. 1(b). Validation requires that similar trends with respect to chain architecture are obtained for both fine grained (MD) and coarse grained (DPD) simulation.

5. Conclusion

Pore morphologies within meso phase separated hydrated grafted polymeric membranes were simulated by DPD in which polymer fragments are represented by connected beads. Water diffusion through the water containing pores was modeled separately by means of MC tracer calculations through selected (static) morphologies. Four types of membranes were considered that are of equal IEC but differ in the way side chains are attached to the hydrophobic backbones. The main and side chains were flexible with no bending stiffness taken into account, therefore the phase separated pore morphologies are solely governed by the adapted Flory-Huggins χ parameters, polymer architecture, and water contents (16 volume %). With A beads being hydrophobic and C beads hydrophilic, it was found that for polymers composed of similar length of 24 backbone beads the MC derived diffusion constants through static (frozen) pore networks increase as A4[AC] < A7[AC]A1[AC] < A8[A2C2] < A8[AC][AC]. Simulations performed for the A8[A2C2] and A8[AC][AC] architectures of two times longer length (48 backbone beads), revealed again the A8[AC][AC] polymer showing the highest water diffusion constant of both.

The results are complemented by calculation of diffusion of the water beads through the evolving dynamic DPD pore network. The same trend as derived from the MC calculations was obtained with water diffusion being systematically higher for the A8[AC][AC] architecture. This trend turned not be affected when the mobility of the polymer A and/or C beads was artificially decreased by increase of the bead masses. These new insights suggests that within (new types of) membranes of equal IEC but with two side chains branching off from a single backbone site allows the formation of better connected hydrophilic pores.

References

[1] G.M. Geise, H.S. Lee, D.J. Miller, F.D. Freeman, J.E. McGrath, D.R. Paul, J. Polym. Sci. B Polym. Phys. 48 (2010) 1685–1718.
[2] M. Saito, N. Arimura, K. Hayamizu, J. Okada, Phys. Chem. B 108 (2004) 16064–16070.
[3] T.A. Zawodzinski Jr., C. Derouin, S. Radzinski, R.J. Sherman, V.T. Smith, T.E. Springer, S. Gottesfeld, J. Electrochem. Soc. 140 (1993) 1041–1047.
[4] J.T. Hinatsu, M. Mizuhata, H. Takenaka, J. Electrochem. Soc. 141 (1994) 1493–1498.
[5] Q. Zhao, N. Carro, Y.R. Ho, J. Benziger, Polymer 53 (2012) 1267–1276.
[6] M. Bass, V. Freger, Polymer 49 (2008) 497–506.
[7] T.D. Gierke, G.E. Munn, F.C. Wilson, J. Polym. Sci. Polym. Phys. 19 (1981) 1687–1704.
[8] K.A. Mauritz, R.B. Moore, Chem. Rev. 104 (2004) 4535–4585.
[9] K. Schmidt-Rohr, Q. Chen, Nat. Mater. 7 (2008) 75–83.
[10] C.A. Edmonson, J.J. Fontanella, Solid State Ionics 152–153 (2002) 355–361.
[11] K.D. Kreuer, M. Schuster, B. Obliers, O. Diat, U. Traub, A. Fuchs, U. Klock, S.J. Padisson, J. Maier, J. Power Sources 178 (2008) 499–509.
[12] Q. Li, R. He, J.O. Jensen, N.J. Bjerrum, Fuel Cells 4 (2004) 147–159.
[13] X.P. Xing, G.P. Robertson, M.D. Guiver, S.D. Mikhailenko, K.P. Wang, S. Kaliaguine, J. Membr. Sci. 229 (2004) 95–106.
[14] X. Li, C. Zhao, H. Lu, Z. Wang, H. Na, Polymer 46 (2005) 5820–5827.
[15] N. Li, D.W. Shin, D.S. Hwang, J.M. Lee, M.D. Guiver, Macromolecules 43 (2010) 9810–9820.
[16] M. Lee, J. Park, H.-S. Lee, O. Lane, R.B. Moore, J.E. McGrath, D.G. Baird, Polymer 50 (2009) 6129–6138.
[17] K. Miyatake, H.Z. Zhou, T. Matsuo, H. Uchida, M. Watanabe, Macromolecules 37 (2004) 4961–4966.
[18] C.H. Park, C.H. Lee, J.-H. Sohn, H.B. Park, M.D. Guiver, J.M. Lee, J. Phys. Chem. B 114 (2010) 12036–12045.
[19] J.R. Atkins, C.R. Sides, S.E. Creager, J.L. Harris, W.T. Pennington, B.T. Thomas, D.D. DesMarteau, J. New. Mater. Electrochem. Syst. 6 (2003) 9–15.
[20] J.A. Elliot, S. Hanna, A.M.S. Elliot, G.E. Cooley, Phys. Chem. Chem. Phys. 1 (1999) 4855–4863.
[21] A. Vishnyakov, A.V. Neimark, J. Phys. Chem. B 105 (2001) 9586–9594.
[22] R. Jinnouchi, K. Okazaki, J. Electrochem. Soc. 150 (2003) E66–E73.
[23] D. Seeliger, C. Hartnig, E. Spohr, Electrochim. Acta 50 (2005) 4234–4240.
[24] S. Urata, J. Irisawa, A. Takada, W. Shinoda, S. Tsuzuki, M. Mikami, J. Phys. Chem. B 109 (2005) 4269–4278.
[25] X. Zhou, Z. Chen, F. Delgado, D. Brenner, R.J. Srivastava, J. Electrochem. Soc. 154 (2007) B82–B87.
[26] S. Cui, J. Liu, M.E. Selvan, S.J. Paddison, D.J. Keffer, B.J. Edwards, W.V. Steele, J. Phys. Chem. B 111 (2007) 2208–2218.
[27] R. Devanathan, A. Venkatnathan, R. Rousseau, M. Dupuis, T. Frigato, W. Gu, V. Helms, J. Phys. Chem. B 114 (2010) 13681–13690.
[28] S. Cui, J. Liu, M.E. Selvan, S.J. Paddison, D.J. Keffer, B.J. Edwards, J. Phys. Chem. 112 (2008) 13273–13284.
[29] J. Karo, A. Aabloo, J.O. Thomas, D. Brandell, J. Phys. Chem. B 114 (2010) 6056–6064.
[30] D. Brandell, J. Karo, A. Liivat, J.O. Thomas, J. Mol. Model 13 (2007) 1039–1046.
[31] C.K. Knox, G.A. Voth, J. Phys. Chem. B 114 (2010) 3205–3218.
[32] S.S. Jang, V. Molinero, T. Cagin, W.A. Goddard III, J. Phys. Chem. B 108 (2004) 3149–3157.
[33] W. Allahyarov, P. Taylor, J. Polym. Sci. B Polym. Phys. 49 (2011) 368–376.
[34] G. Dorenbos, Y. Suga, J. Membr. Sci. 330 (2009) 5–20.
[35] G. Dorenbos, K. Morohoshi, Energy Environ. Sci. 3 (2010) 1326–1338.
[36] G. Dorenbos, V.A. Pomogaev, M. Takigawa, K. Morohoshi, Electrochem. Comm. 12 (2010) 125–128.

[37] G. Dorenbos, K. Morohoshi, J. Chem. Phys. 134 (2011) 044133.
[38] G. Dorenbos, K. Morohoshi, J. Mater. Chem. 21 (2011) 13503–13515.
[39] G. Dorenbos, K. Morohoshi, J. Chem. Phys. 138 (2013) 064902.
[40] G. Dorenbos, RSC Adv. 3 (2013) 18630–18642.
[41] G. Dorenbos, Polymer 54 (2013) 5024–5034.
[42] S. Yamamoto, S.-A. Hyodo, Polym. J. 35 (2003) 519–527.
[43] N.A. Spenley, Europhys. Lett. 49 (4) (2000) 534–540.
[44] P.J. Hoogerbrugge, J.M.V.A. Koelman, Europhys. Lett. 19 (1992) 155–160.
[45] R.D. Groot, T.J. Madden, J. Chem. Phys. 108 (1998) 8713–8724.
[46] R.D. Groot, K.L. Rabone, Biophys. J. 81 (2001) 725–736.
[47] S. Yamamoto, Y. Murayama, S. Hyodo, J. Chem. Phys. 116 (2002) 5842–5849.
[48] H. Wang, Y.-T. Liu, H.-J. Qian, Z.-Y. Lu, Polymer 52 (2011) 2094–2101.
[49] X.D. Guo, L.J. Zhang, Z.M. Wu, Y. Qian, Macromolecules 43 (2010) 7839–7844.
[50] R.D. Groot, P.B. Warren, J. Chem. Phys. 107 (1997) 4423–4435.
[51] P. Espanol, P. Warren, Europhys. Lett. 230 (1995) 191–196.
[52] W. Humphrey, A. Dalke, K. Schulten, J. Mol. Graph. 14 (1) (1996) 33–38.
[53] Z. Ogumi, T. Kuroe, Z. Takehara, J. Electrochem. Soc. 132 (1985) 2601–2605.
[54] H.F.M. Mohamed, Y. Kobayashi, C.S. Kuroda, A. Ohira, J. Phys. Chem. B 113 (2009) 2247–2252.
[55] H.-G. Haubold, Th Vad, H. Jungbluth, P. Hiller, Electrochim. Acta 46 (2001) 1559–1563.
[56] J.-C. Perrin, S. Lyonnard, F. Volino, J. Phys. Chem. C 111 (2007) 3393–3404.
[57] A.M. Pivovar, B.S. Pivovar, J. Phys. Chem. B 109 (2005) 785–793.
[58] M. Webber, N. Dimakis, D. Kumari, M. Fuccillo, E.S. Smotkin, Macromolecules 43 (2010) 5500–5502.
[59] J.A. Elliot, S.J. Paddison, Phys. Chem. Chem. Phys. 9 (2007) 2602–2618.
[60] P.V. Komarov, P.G. Khalatur, A.R. Khoklov, J. Nanotechnol. 4 (2013) 567–587.